ENDMEMBER SET SELECTION FOR HYPERSPECTRAL IMAGERY

Nareenart Raksuntorn

Lecture, the Faculty of Industrial Technology, Suansunandha Rajabhat University,

1 U-Thongnok Road, Vajira, Dusit, Bangkok, 10300, Thailand;
Tel: +66(0) – 2160 – 1431; Fax: +66(0) – 2160 – 1440
E-mail: nareenart@ssru.ac.th

KEY WORDS: Linear mixture model, multiple endmember spectral mixture analysis, hyperspectral imagery

Abstract: Linear mixture model (LMM) is widely used in remote sensing data. It requires the number of endmembers and their signatures. Endmember signature matrix used in LMM is the same for the entire process, which may not be true when the image scene is large. The multiple endmember spectral mixture analysis (MESMA) has been proposed to relax the limitation of LMM, i.e., the number of endmembers and their types can be changed from pixel to pixel. For a given pixel, MESMA searches for the endmember set from all the endmembers present in the image scene. In this paper, MESMA is referred to as endmember-variable LMM (EVLMM). This algorithm is particularly designed for hyperspectral imagery. There is no need any threshold requirements in the searching process. In fact, the computational complexity of searching process increases as the number of endmembers increases. A challenging problem is to reduce the computational complexity of searching process when the number of endmembers is high. In this paper, we present an algorithm to fasten the searching process in EVLMM. The algorithm first divides the original image into sub-images and then performs EVLMM for the individual sub-image. A sub-image endmember set (Sub-ES) consists of endmembers located in the sub-image and their neighbors chosen from endmember distances. The image endmember set (ES) or Sub-ES is selected for a given pixel based on its spatial information. In general, pixels with similarly spatial information are most likely made from the same endmember set. Hence, the Sub-ES is chosen for these pixels and the ES is preferred for the others. An experimental comparison of the original and proposed algorithms is conducted. The result demonstrates that the proposed algorithm speeds up the searching process while retaining the quality of estimated abundances.

1. INTRODUCTION

A hyperspectral image sensor employs hundreds of spectral channels to collect data for an area of interest. The example of hyperspectal image sensor includes the Airborn Visible/Infrared Imagine Spectrometer (AVIRIS), Hyperspectral Digital Imagery Collection Experiment (HYDICE), and the space borne Hyperion. The AVIRIS image contains 224 contiguous spectral bands ranging from 400 to 2,500 nm with 20 m spatial resolution and 10 nm spectral resolution while the HYDICE has 210 spectral bands with the same spectral band and spatial resolution between 0.75 and 3.75 m. Hyperion sensor collects 224 spectral bands with 30 m spatial resolution and 10 nm spectral resolution. Due to the rough spatial resolution, more than one material may be resident in the area covered by a pixel. In such case, a pixel can be considered as the mixture of pure materials.

The linear mixture model (LMM) describes a pixel as a linear combination of endmember signatures and their abundances as follows.

$$\mathbf{r} = \mathbf{M}\boldsymbol{\alpha} + \mathbf{n}, \tag{1}$$

where $\mathbf{r}$ is $L \times 1$ column pixel vector with L being the number of spectral bands, $\mathbf{M} = [\mathbf{m}_1, \mathbf{m}_2, \ldots, \mathbf{m}_p]$ is the endmember signature matrix containing p endmembers, $\boldsymbol{\alpha} = (\alpha_1, \alpha_2, \ldots, \alpha_p)^T$ is the abundance vector with α_j being the abundance fraction of $\mathbf{m}_j$ present in $\mathbf{r}$, and $\mathbf{n}$ is an additive noise. When the number of endmembers and their signatures are known, least squares (LS) approach can be used to estimate the abundances such that the pixel reconstruction error is minimized, i.e.,

$$\min_{\hat{\alpha}} \|$$

The estimated abundance solved by eq.(3) can be non-negative values due to mathematical calculation. To satisfy physical meaning, abundances in each pixel should be non-negative numbers and the abundance sum must equal to one, i.e., (Shimabukuro & Smith, 1991)

$$\sum_{j=1}^{p} \alpha_j = 1 \text{ and } \alpha_j \geq 0. \quad (4)$$

The fully constrained least squares linear unmixing (FCLS) proposed in (Heize & Chang, 2001) is one approach to estimate the abundances under the two constraints. However, reinforcing the abundance constraints may yield erroneous results (Elmore, *et. al*., 2000). Multiple endmember spectral mixture analysis (MESMA) was proposed in (Robert, *et. al*., 1992) for multispectral endmember set selection, where the number of endmembers and their types can vary from pixel to pixel for the entire image. In the searching step, MESMA searches for endmember sets that meet the criteria and selects the endmember set that produces the minimum pixel reconstruction error as the actual endmember set (AES) for a given pixel. MESMA requires a preset threshold for the criteria; therefore, the accuracy is actually based on user's experience. Later, the endmember-variable LMM (EVLMM) was proposed particularly for hyperspectral images, where no threshold is needed. The details will be described in next section.

2. THEORETICAL BACKGROUND

To apply LMM when there is no prior information about the image scene, the number of endmembers is a first requirement. This number can be estimated by the number of endmembers estimation techniques. After the number of endmembers is known, the next step is to identify endmember signatures according to the estimated number of endmembers. When it is assumed that there are pure pixels in the image scene, endmember signatures can be extracted by endmember extraction techniques. Once the number of endmembers and their signatures are found, LMM or EVLMM can be applied. In this section, we briefly describe some related work including spatial information, virtual dimensionality (VD), unsupervised FCLS (UFCLS), and EVLMM algorithms. The detailed are given below.

Spatial Information

Spatial homogeneity index illustrates how similarity between a given pixel in the original image and its neighbors. A lower spatial homogeneity index implies that a given pixel and its neighbors are more similar and vice versa. This index is calculated by (Martin & Plaza, 2012)

$$\text{RMSE}[\mathbf{r}(i,j), \mathbf{r}'(i,j)] = (\sum_{l=1}^{L}(\mathbf{r}_l(i,j) - \mathbf{r}'_l(i,j))^2)^{1/2}, \quad (5)$$

where $\mathbf{r}(i,j)$ is an image pixel, $\mathbf{r}'(i,j)$ is the corresponding filtered image pixel, l is the l-th band with $1 \leq l \leq L$, and L is the number of bands. Here, Gaussian filtering is applied to the original image for the filtered image.

VD Algorithm

The VD algorithm has succeeded in estimating the number of endmembers in many applications. It requires a false alarm rate, P_F, to control its estimation. VD is based on the eigenvalues of the sample correlation and covariance matrices. The difference between the correlation eigenvalue, $\hat{\lambda}_l$, and covariance eigenvalue,λ_l , is used to determine the number of endmembers. If $\hat{\lambda}_l - \lambda_l > 0$, means there is signal variance contributing to the correlation eigenvalues of the l-th band since noise eigenvalue of the correlation and the corresponding eigenvalue of the covariance are equal. To determine the number of endmembers, the problem can be formulated as follows (Harsanyi *et. al.*, 1994).

$$H_0: z_l = \hat{\lambda}_l - \lambda_l = 0 \quad \text{and} \quad H_1: z_l = \hat{\lambda}_l - \lambda_l > 0.$$

The P_F and detection probability, P_D, are defined as the following

$$P_F = \int_{\tau_l}^{\infty} p_0(z)dz \quad \text{and} \quad P_D = \int_{\tau_l}^{\infty} p_1(z)dz,$$

where τ_l is a detection threshold.

UFCLS Algorithm

The UFCLS algorithm is one of endmember extraction techniques. The basic idea is to find a set of pixels such that each pixel in this set is most dissimilar to the others based on the linear unmixing error. The details are described as follows.

1. A pixel with the maximum length is selected as an initial endmember signature $\mathbf{m}_0$. The abundance α_0 for each pixel in this case is one.
2. Search for a pixel $\mathbf{r}$ that has the maximum error between the pixel and its reconstruction and define it as the first endmember $\mathbf{m}_1$. The endmember signature matrix $\mathbf{M} = [\mathbf{m}_1]$.
3. Calculate the error between the pixel $\mathbf{r}$ and its estimate. The pixel $\mathbf{r}$ with the maximum error is selected as the second endmember $\mathbf{m}_2$, and it is concatenated to the endmember signature matrix, i.e., $\mathbf{M} = [\mathbf{m}_1\ \mathbf{m}_2]$, and then estimate the corresponding abundance $[\alpha_1\ \alpha_2]$ using the FCLS (Heize & Chang, 2001).
4. Repeat step 4 until p endmembers are found.

EVLMM Algorithm

This algorithm assumes that there is an optimal endmember set for a given pixel. In general, the MSE depends on the number of endmembers; the larger the number of endmembers, the smaller MSE on the reflectance reconstruction. So, the algorithm will search for the combinations with fewer endmembers that produces all nonnegative abundances and the smallest MSE on the reflectance reconstruction. EVLMM algorithm can be summarized as follows.

1. Normalize pixel vectors and all the endmember signatures to ensure that the abundances obtained from LS are not dominated by their high energy, to which the MSE is sensitive. For example, if a less-significant endmember with a higher energy is removed from the endmember set, the corresponding MSE may be larger, which introduces an inaccurate endmember set.
2. Determine the abundances using the endmembers in the initial endmember set (IES) with the LS. If the abundances are all nonnegative values, the IES is kept as the AES. If there is one or more negative abundances, go to the next step.
3. Find the abundances from the combinations with one endmember, apply the LS, and then calculate the MSE. Keep the combination that produces all nonnegative abundances with the minimum MSE.
4. Repeat Step 3 by searching from the two-endmember combinations. If the minimum MSE in the current step is greater than that in the previous step, the combination obtained from the previous step is selected as the ASE and the algorithm is terminated. Otherwise, test the combinations with more endmembers.

3. PROPOSED APPROACH

In this section, we present an algorithm, called FEVLMM, to fasten the searching step in EVLMM proposed in (Raksuntorn & Du, 2008). The number of endmembers in the image scene is determined by the VD estimation with $P_F = 10^{-4}$. Endmembers are extracted by the UFCLS technique. All extracted endmembers will be in the image endmember set (ES). The proposed algorithm shown in Figure 1 consists of three major steps as given below.

Image Division

In this step, the image scene is divided into non-overlapping sub-images. Endmembers extracted by the UFCLS located in sub-image are designed as the Sub-ES. A sub-image size depends on the entire image and its complexity. If the image is highly mixed, a smaller sub-image size would provide a better result. However, too small sub-image size leads the more non-homogeneity pixels in the sub-image, which increases the computational time.

Spatial Information

In this step, spatial homogeneity index calculated by the method in (Martin & Antonio, 2012) is used to determine pixel homogeneity. Pixels in homogenous area are more likely constructed by the same endmember set. Hence, these pixels are to search for their endmember sets from the Sub-ES while the ES is applied for the other pixels.

Endmember Distance

The distance between endmembers located in the sub-image and adjacent sub-image are calculated. If the distance is below a predefined threshold, the endmember in the adjacent sub-image is added into the sub-ES. The average distance can be defined as a predefined threshold.

In summary, we first divide an image scene into sub-images. A Sub-ES of each sub-image consists of the endmembers located in the sub-image and the endmembers obtained from the adjacent sub-images with the distance below the predefined threshold. For each sub-image, Sub-ES is assigned for pixels in homogeneity area, and ES is selected for the other pixels. More pixels in homogenous area mean less computational time consuming in the searching step.

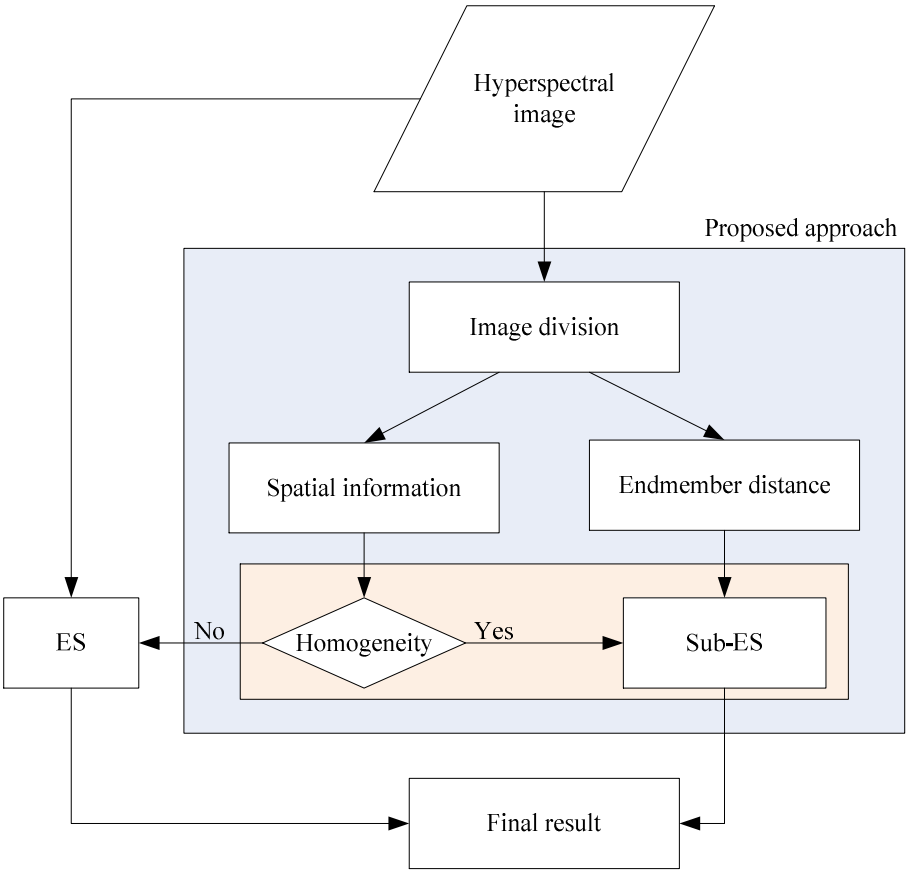

Figure 1 Block diagram of the proposed approach

4. EXPERIMENTS

The Airborne Visible InfraRed Imaging Spectrometer (AVIRIS) data set was used in this experiment. The image scene was taken from the Lunar Crater Volcanic Field in Northern Nye County, Nevada, with 200 × 200 pixels and 158 bands after low signal-to-noise ratio (SNR) and water absorption bands were removed. This image scene was well studied. There are at least five materials including cinder, playa, rhyolite, shade, and vegetation. In addition, there is an anomaly pixel in the image scene. The Lunar lake image scene was shown in Figure 2.

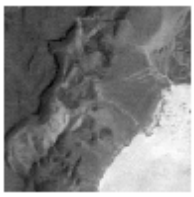

Figure 2 Lunar Lake (Band 100)

In the experiment, the estimate of the number of endmembers was six. Six endmembers were extracted by the UFCLS algorithm. These endmembers were considered as the ES. The image scene was divided into four non-overlapping sub-images with a size of 100 × 100 pixels and 158 bands. The homogeneity index threshold was set to the difference between the mean and variance of the distances. For each sub-image, the predefined distance threshold was set to the average distance between all the endmembers located in the sub-image and the adjacent sub-images. All experiments were run by the personal computer (PC) with 1.6GHz CPU and 2GB memory. Figure 3 illustrates the abundance maps after applying the FCLS, EVLMM, and FEVLMM. It can be seen that the abundance maps obtained from the proposed technique were similar to that from the FCLS and EVLMM.

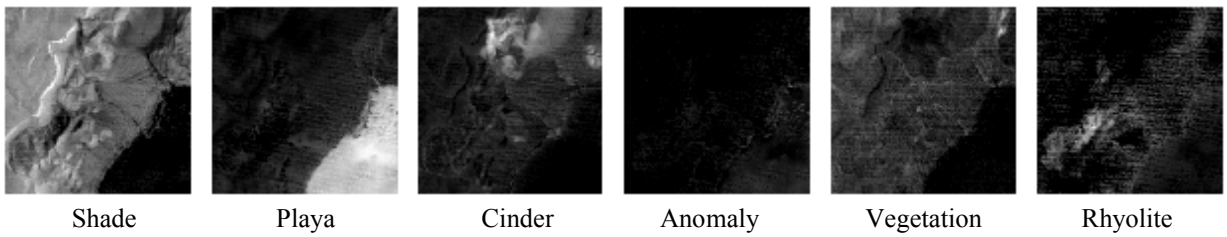

Shade Playa Cinder Anomaly Vegetation Rhyolite

(a) FCLS

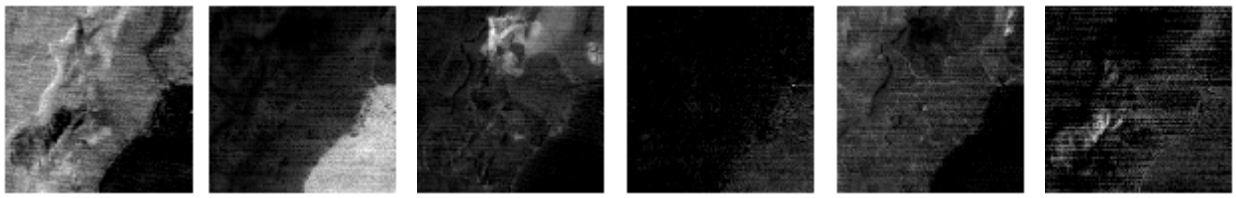

Shade Playa Cinder Anomaly Vegetation Rhyolite

(b) EVLMM

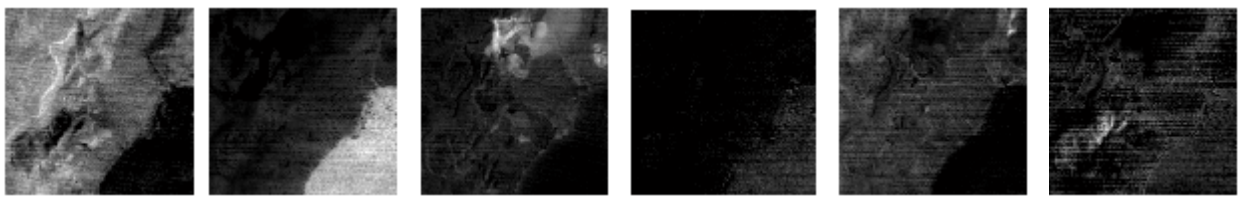

Shade Playa Cinder Anomaly Vegetation Rhyolite

(c) FEVLMM

Figure 3 Abundance Maps using the FCLS, EVLMM, and FEVLMM

Table 1 lists the MSE between pixels and their estimates and the runtime. We can see that the MSEs from the EVLMM and FEVLMM were less than that from the FCLS while the FEVLMM yielded a slightly greater MSE than EVLMM. When compare the runtime, FEVLMM took about 420 seconds; EVLMM spent about 540 seconds; and FCLS needed about 534 seconds. It is obvious that the FEVLMM produced a minimum runtime following by the EVLMM and FCLS, respectively.

Table 1 The MSE on reflectance and runtime

Method	MSE	Runtime (second)
FCLS	76.4874	534.1739
EVLMM	73.0694	539.5117
FEVLMM	73.4368	420.0353

Table 2 lists the percentage of pixels with abundance sums. The abundances of all pixels from the three algorithms were non-negative. For FEVLMM, 99.45% of pixels had the abundances whose sums were between 0.8 and 1.2. When the range was decreased to [0.85 1.15] and [0.9 1.1], the percentages were about 96.46% and 83.05%, respectively. The EVLMM results were slightly better than FEVLMM; 99.52% of pixels had the abundances whose sums were between 0.8 and 1.2. When the range was decreased to [0.85 1.15] and [0.9 1.1], the percentages were about 96.85% and 84.47%, respectively. All abundance sums from the FCLS were equal to one since the two constraints were imposed.

Table 2 The percentage of pixels with abundance sums

Method	Range of 0.80 - 1.20 (%)	Range of 0.85 - 1.15 (%)	Range of 0.90 - 1.10 (%)
FCLS	100	100	100
EVLMM	99. 5175	96.8475	84.4650
FEVLMM	99. 4525	96.4550	83.0525

Table 3 lists the residual counts produced by the three algorithms. In this experiment, a residual count is the number of pixels from which this technique yields individual errors more than a preset threshold, T. For all thresholds, FCLS yielded the largest residual counts following by EVLMM and FEVLMM, respectively. We can see that the residual counts produced by FEVLMM were slightly greater than that from EVLMM. Over all, the execution time of FVELMM was the shortest while its performance on the abundances and the residual counts was slightly lower than that from EVLMM.

Table 3 The residual counts

Method	$T = 50$	$T = 60$	$T = 70$
FCLS	2520	495	88
EVLMM	1499	239	25
FEVLMM	1603	263	32

5. CONCLUSIONS

The EVLMM was developed for determining a realistic endmember set for a given pixel without any threshold requirements. EVLMM algorithm was useful and effective in selecting an optimal or sub-optimal endmember set, i.e., the sum-to-one and non-negativity constraints on the abundances were automatically satisfied. The MSE and residual counts on pixel reconstruction is less than that of the FCLS. The computational complexity depends on the number of endmembers. When the number of endmembers is large, the searching step is computationally expensive due to too many combinations.

This paper presents an algorithm to fasten the searching process in the EVLMM, called FEVLMM. The original image was divided into sub-images. Sub-image endmember set consists of endmembers located in the sub-image and selected neighboring endmembers. Obviously, each sub-image contained less the number of endmembers than that of the original image. So, the computational complexity was greatly decreased in the implementation. The results showed that the proposed algorithm speeded up the searching process in the EVLMM. The performances on

the MSE and residual counts on pixel reconstruction of the original and proposed algorithms were quite similar. There is a traded off between the performance and computational complexity; the lower threshold in neighboring endmember selection, the higher the number of endmembers in the sub-image endmember set and the higher computational complexity. Future work includes investigating of methods to the choice of homogeneity index threshold and the combining between spectral similarity and spatial information used in the neighboring endmember selection.

ACKNOWLEDGEMENT

This research was supported by Suansunandha Rajabhat University, Thailand. The author would like to thank Dr. Jenny Du for providing the data used in the experiment. The author would also like to thank Dr. Antonio Plaza for providing the code used to define the homogeneity index.

REFERENCES:

Elmore, A. J., Mustard, J. F., Manning, S. J., and Lobell, D. B., 2000. Quantifying vegetation change in semiarid environments: precision and accuracy of spectral mixture analysis and the normalized difference vegetation index. Romote Sensing Environment, 73 (1), pp. 87-102.

Harsanyi, J., and Chang, C.-I., 1994. Hyperspectral image classification and dimensionality reduction: an orthogonal subspace projection approach. IEEE Transaction on Geoscience. Remote Sensing, 32 (4), pp.779-785.

Heize, D., and Chang, C.-I., 2001. Fully constrained least squares linear mixture analysis for material quantification in hyperspectral imagery. IEEE Transaction on Geoscience. Remote Sensing, 39 (3), pp. 529-545.

Martin, G. and Plaza, A., 2012. Spatial-Spectral Preprocessing prior to endmember identification and unmixing of remotely sensed hyperspectral data. Journal of Selected Topics in Applied Earth Observations and Remote Sensing, 5 (2), pp. 380-395.

Raksuntorn, N. and Du, Q., 2008. A new linear mixture model for hyperspectral image analysis. Proceedings of IEE Geoscience and Remote Sensing Symposium, 3, pp. 258-261.

Roberts, D. A., Smith, M. O., Sabol, D. E., Adams, J. B., and Ustin, S., 1992. Mapping the spectral variability in photosynthetic and non-photosynthetic vegetation, soils and shade using AVIRIS. Summaries of 3rd Annual JPL Airborne Geoscience Workshop, pp. 38-40.

Shimabukuro, Y. E., and Smith, J. A., 1991. The least-squares mixing models generate fraction images derived from remote sensing multispectral data. IEEE Transaction on Geoscience. Remote Sensing, 29 (1), pp. 16-20.